Research Square

Preprints are preliminary reports that have not undergone peer review.
They should not be considered conclusive, used to inform clinical practice,
or referenced by the media as validated information.

Seasonality controls on Last Glacial Maximum glacier dynamics in the southern European Alps

Lukas Rettig

rettig@vaw.baug.ethz.ch

Swiss Federal Institute of Technology Zürich (ETHZ) https://orcid.org/0000-0002-8242-3386

Giovanni Monegato

Institute of Geosciences and Earth Resources, National Research Council of Italy

Matteo Spagnolo

Department of Earth Sciences, University of Turin

Brice Rea

University of Aberdeen https://orcid.org/0000-0002-9928-145X

Sarah Kamleitner

Institute of Earth Surface Dynamics, University of Lausanne

Costanza Del Gobbo

Istituto di Scienze Polari, Venezia

Susan Ivy-Ochs

ETH Zürich, Laboratory of Ion Beam Physics https://orcid.org/0000-0002-3242-9536

Adriano Ribolini

Department of Earth Sciences, University of Pisa

Franco Gianotti

Department of Earth Sciences, University of Turin

Marcus Christl

ETH Zürich https://orcid.org/0000-0002-3131-6652

Christof Vockenhuber

Swiss Federal Institute of Technology in Zurich https://orcid.org/0000-0002-2141-0733

Paolo Mozzi

University of Padua

Article

Keywords:

Posted Date: March 12th, 2026

DOI: https://doi.org/10.21203/rs.3.rs-8895450/v1

License: This work is licensed under a Creative Commons Attribution 4.0 International License.
Read Full License

Additional Declarations: There is **NO** Competing Interest.

Seasonality controls on Last Glacial Maximum glacier dynamics in the southern European Alps

Lukas Rettig[1,2,3] (*), Giovanni Monegato[4], Matteo Spagnolo[5], Brice R. Rea[6], Sarah Kamleitner[7,8], Costanza del Gobbo[9], Susan Ivy-Ochs[7], Adriano Ribolini[10], Franco Gianotti[5], Marcus Christl[7], Christof Vockenhuber[7], Paolo Mozzi[1]

[1]Department of Geosciences, University of Padua, Italy. [2]Laboratory of Hydraulics, Hydrology and Glaciology (VAW), ETH Zürich, Zürich, Switzerland. [3]Swiss Federal Institute for Forest, Snow and Landscape Research (WSL), Bâtiment ALPOLE, Sion, Switzerland. [4]Institute of Geosciences and Earth Resources, National Research Council of Italy, Padua, Italy. [5]Department of Earth Sciences, University of Turin, Italy. [6]Department of Geography and Environment, School of Geosciences, University of Aberdeen, United Kingdom. [7]Laboratory of Ion Beam Physics, ETH Zürich, Zürich, Switzerland. [8]Institute of Earth Surface Dynamics, University of Lausanne, Switzerland. [9]Department of Earth and Atmospheric Sciences, University of Quebec in Montreal, Canada. [10]Department of Earth Sciences, University of Pisa, Italy. (*) Corresponding author (rettig@vaw.baug.ethz.ch).

Abstract: Glaciers in mountain ranges across Europe reached their local Last Glacial Maximum (l-LGM) extent at different times throughout the last glacial cycle, yet the causes of this asynchronous behaviour remain incompletely understood. Here, we propose precipitation seasonality as a key control for this phenomenon. The hypothesis is based on an internally coherent reconstruction of 16 l-LGM mountain glaciers and their Equilibrium Line Altitudes (ELAs) along the southern margin of the European Alps. ^{10}Be and ^{36}Cl surface exposure dating in selected catchments demonstrates that these marginal glaciers had advanced to their l-LGM positions by 25 to 24 ka, where they remained until ca. 19 ka. By combining the empirical reconstructions with outputs from a regional palaeoclimate model, we show that glacier mass balance during this period was strongly influenced by snowfall not only in winter but also during autumn and spring to early summer. This specific precipitation seasonality distinguished glaciers in the southern Alps from mountain glaciers elsewhere in southern Europe that were mainly fed by winter precipitation and faced widespread retreat after 25 ka under increasingly arid conditions. Spring and autumn snowfall along the Alpine fringe could buffer the effects of increasing aridity and allowed Alpine glaciers to remain at or close to their maximum extent also after 25 ka.

Accurately constraining climatic controls on mountain glacier evolution during past cold periods is essential for predicting their future fate under global warming (Mackintosh et al., 2017; Hock et al., 2019). The Last Glacial Maximum (LGM) was one of the most significant climatic events in the Earth's more recent history. Characterised by a pronounced atmospheric cooling during the early part of Marine Isotope Stage 2 (MIS 2, 29-14 ka), the LGM saw the expansion of continental ice sheets in the Northern Hemisphere, which in turn resulted in a global sea level lowstand (Fig. 1A; Ehlers et al., 2011; Lambeck et al., 2014). The period of maximum integrated ice volume and minimum sea level, i.e. the global (g-)LGM, occurred between ca. 26.5 and 19 ka, and mainly coincides with the largest extent of the Laurentide ice sheet (Clark et al., 2009). At the regional scale, however, there is growing evidence that local LGM (l-LGM) maxima were reached asynchronously and often out-of-phase with the (g-)LGM (Gillespie and Molnar, 1995; Hughes et al., 2013).

This asynchrony was especially pronounced in mountain ranges across Europe, many of which hosted glaciers and small ice caps throughout the last glacial cycle (Fig. 1B; Palacios et al., 2021; López-Moreno and García-Ruiz, 2025). The biggest ice extent in central Europe (e.g., in the Vosges, the Tatras, or the Romanian Carpathians) occurred predominantly in-phase with the g-LGM (Reuther et al., 2011; Engel et al., 2015; Makos et al., 2018). By contrast, many mountain glaciers in southern Europe (e.g., in the Pyrenees, the central Apennines, and the southern Balkans) appear to have reached their maxima much earlier, either already during MIS 3 (57-29 ka) or during the early part of MIS 2, before 25 ka (Delmas et al., 2011; Giraudi, 2012; Allard et al., 2020; Allard et al., 2021; Ribolini et al., 2022a). This asynchronous behaviour signals that European glaciers often responded to specific regional and local conditions that modulated a global climatic forcing. Palaeoclimatic variations at these small spatial scales, however, have remained poorly resolved, partly because they are hardly captured by global circulation models (GCMs) that run with coarse resolutions. Improvements of regional climate models (RCMs), and their application in a paleoclimatic framework have lately yielded more detailed insights into temperature, precipitation and atmospheric circulation patterns at regional and local scales (Giorgi et al., 2012; Del Gobbo et al., 2023; Russo et al., 2024). Combining the outputs of such RCMs with glacier reconstructions based on empirical, geomorphological and chronological evidence now allows to study climatic controls on LGM glacier mass balance in more detail and to revisit potential explanations for asynchronous ice advances across the continent.

In this context, the southern fringe of the European Alps (from hereon: the southern Alps) represents a key study site, as it is located precisely at the intersection between central and southern Europe (Fig. 1B) - two regions with different climatic regimes and with contrasting chronological data about the LGM glaciation. During the LGM, the Alps hosted a complex and interconnected glacier network, sometimes referred to as the Alpine ice field (AIF, Jouvet et al., 2023; Leger et al., 2025). On the southern side of the AIF (Fig. 1C), large outlet glaciers extended beyond the Alpine fringe, building extensive moraine amphitheatres between ca. 26.5 and 19 ka (Monegato et al., 2007; Monegato et al., 2017; Gianotti et al., 2015; Ivy-Ochs et al., 2018; Braakhekke et al., 2020; Kamleitner et al., 2022). In the lower-elevated pre-Alpine mountains, also numerous marginal mountain glaciers and ice caps developed in isolation from the AIF (Carraro and Sauro, 1979; Baratto et al., 2003; Forno et al., 2010; Monegato, 2012; Rettig et al., 2021; Ribolini et al., 2022b; Rettig et al., 2023;

Rettig et al., 2024). Due to their small size (usually 1-10 km^2), relatively simple catchment geometry, and therefore short response time, these marginal glaciers likely responded rapidly to changes in the LGM climatic forcing (Reuther et al., 2011). They thus represent an ideal target to determine the climatic controls on glacier mass balance and to explore possible explanations for the asynchronous behaviour of mountain glaciers at the continental scale. Yet a regionally coherent analysis of the marginal l-LGM glaciation has never been attempted, and chronological data on these smaller ice masses is still largely lacking (Rettig et al., 2024).

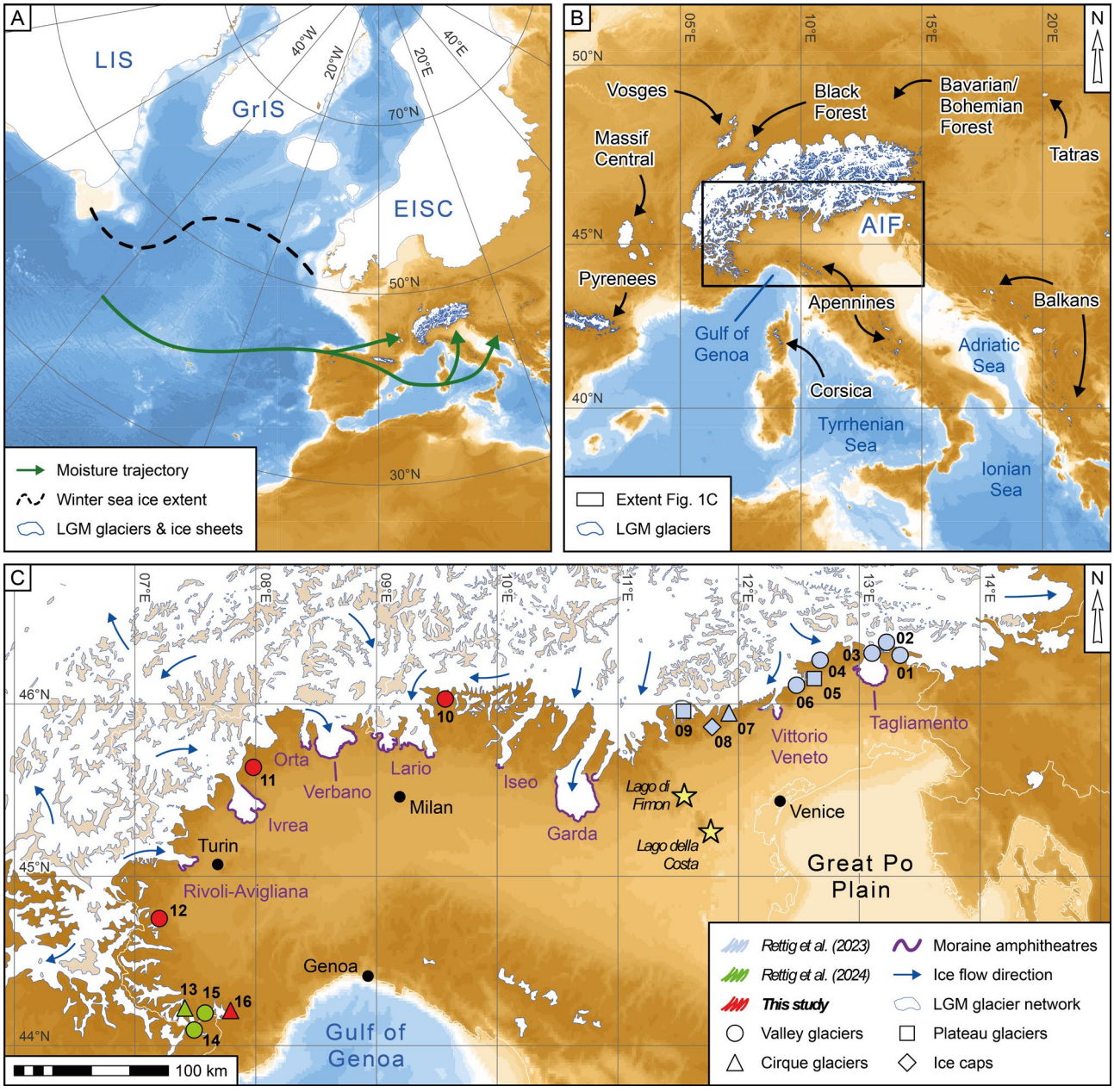


Fig. 1. The southern fringe of the European Alps in the framework of the LGM glaciation. **A.** Atmospheric circulation in the North Atlantic during the g-LGM. Winter sea ice extent and moisture trajectories following Del Gobbo et al. (2023). LIS: Laurentide ice sheet, GrIS: Greenland Ice Sheet, EISC: European ice sheet complex. **B.** Glaciated mountain ranges in central and southern Europe. AIF: Alpine ice field. **C.** Extent of the AIF on the southern side of the Alps, with the locations of major moraine amphitheatres, and marginal palaeoglaciers (numbered from 01 to 16) that were analysed in this study. Source of background DEM and extent of LGM ice sheets (partly updated): Ehlers et al. (2011).

In this study, we provide the first comprehensive reconstruction of marginal l-LGM glaciers along the entire southern fringe of the Alps, integrating previously published data from its south-eastern and south-western sectors (Rettig et al., 2023, 2024) with new findings at four additional field sites (Fig. 1C, Fig. 2, see Supplementary Information). Palaeoglaciers and their Equilibrium Line Altitudes (ELAs) are reconstructed from geomorphological evidence, and ice advances chronologically constrained by ^{10}Be and ^{36}Cl surface exposure dating. Combining our reconstructions with the outputs of an RCM simulating the palaeoclimatic conditions at 21 ka (Del Gobbo et al., 2023), we show that the mass balances of marginal glaciers were strongly impacted by snowfall, not only during winter but crucially also during autumn and late spring/early summer. We propose that this specific precipitation seasonality was a decisive control on the timing of ice advances both in the southern Alps and across Europe and the Mediterranean more broadly.

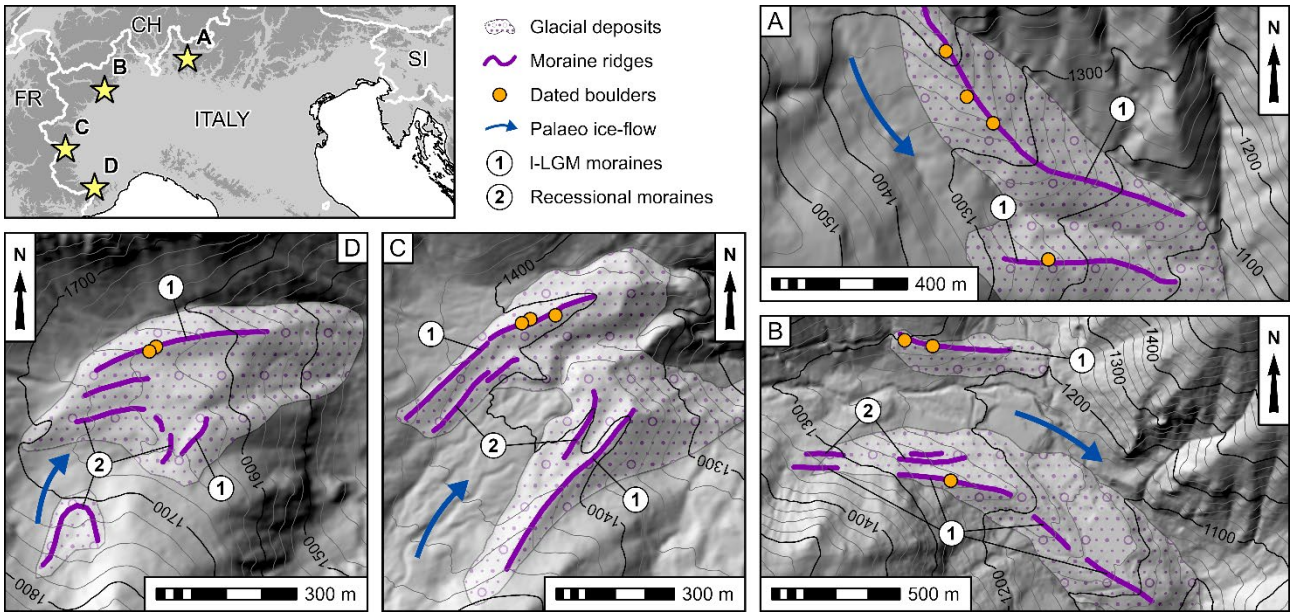


Fig. 2. Newly investigated l-LGM frontal moraine systems related to marginal glaciers along the southern fringe of the Alps. **A**. The lower Inferno Valley (south-central Alps). **B.** The lower Oropa Valley (south- central Alps). **C**. Pian Frollero (south-western Alps). **D.** Sella Spa (south-western Alps). Note in all panels: (1) Prominent l-LGM moraines, and (2) smaller, recessional moraines inside the l-LGM limits. Source of the elevation data: Regione Piemonte (access via: https://www.geoportale.piemonte.it/) and Regione Lombardia (access via: https://irdat.regione.fvg.it/).

Geomorphological evidence of the marginal l-LGM glaciation

Glacial sediments and landforms are preserved in numerous catchments of the pre-Alpine mountains, providing evidence that marginal glaciers existed along the entire southern fringe of the Alps (Fig. 1C). This included both small cirque glaciers, but also more complex plateau glaciers, composite valley glaciers, and local ice caps (Supplementary Information, Table S4). The maximum ice advance (i.e., the l-LGM) is typically marked by a set of large and prominent frontal and lateral moraine ridges (20-50 m high) with well-developed crest lines (Fig. 2). At several sites, smaller recessional moraines (ca. 5 m high) indicate phases of minor readvance and/or stillstand after the glaciers had retreated from their l-LGM positions (Fig. 2). The moraines

generally comprise matrix-supported diamicts containing edge-rounded clasts that exclusively pertain to the local catchment lithologies: carbonates in the south-eastern Alps and magmatic/metamorphic rocks (e.g., gneiss, granite, mica-schist) in the south-central and south-western Alps. The absence of exotic lithologies from the inner-Alpine areas points to proximal sediment sources and demonstrates that marginal glaciers developed in isolation from larger outlet glaciers of the AIF. More detailed information on the morphological evidence at specific sites and on the properties of the reconstructed l-LGM glaciers can be found in Rettig et al. (2023), Rettig et al. (2024), and in the Supplementary Information (Fig. S1-S4).

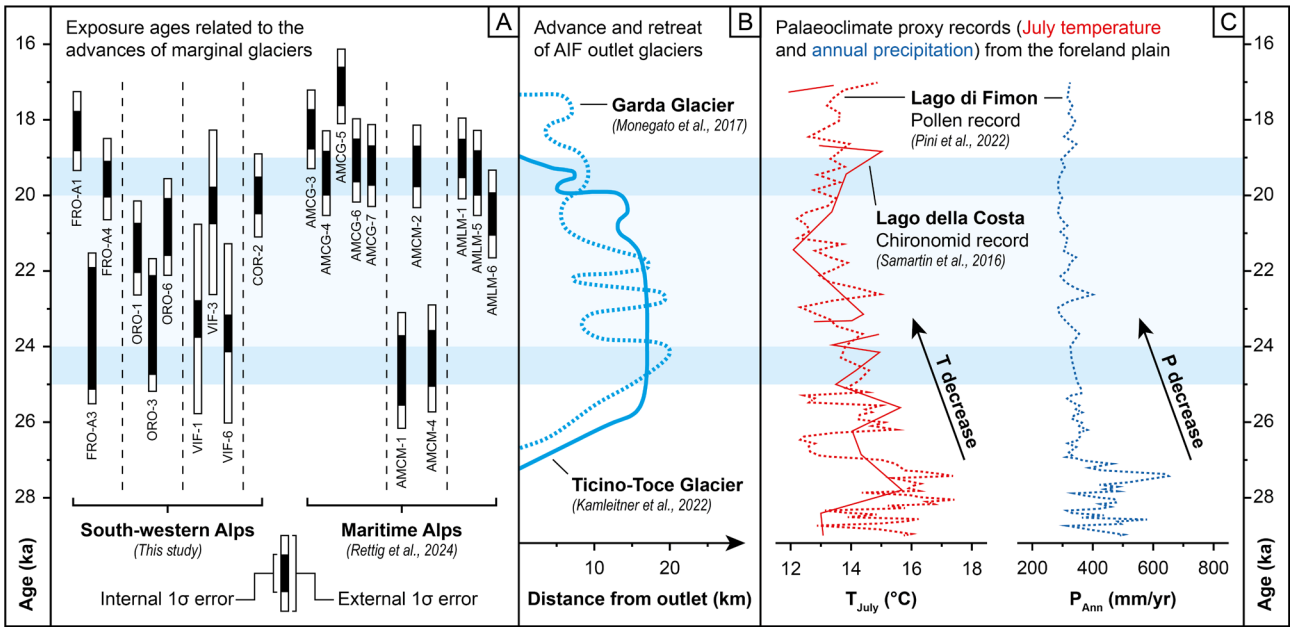


Fig. 3. Chronology of the LGM in the southern Alps. **A.** Surface exposure ages of glacially transported boulders on l-LGM frontal and lateral moraines from the south-western Alps (see Supplementary Information, Table S1 and S2 and Rettig et al., 2024). **B**. Frontal advance and retreat of the Garda and Ticino-Toce outlet glaciers during the LGM (after Monegato et al., 2017; Kamleitner et al., 2022). **C**. Regional palaeoclimate (July temperature and annual precipitation) reconstructions from a chironomid record at Lago della Costa (Samartin et al., 2016) and from a pollen record at Lago di Fimon (Pini et al., 2022). See Fig. 1C for the locations of the outlet glaciers and proxy records. Light blue bars refer to the two main periods of regional ice advance between 25 and 24 and between 20 and 19 ka.

Chronology of moraine formation and ice advances

The advances of marginal glaciers in the southern Alps were chronologically constrained at seven selected sites using ^{10}Be and ^{36}Cl surface exposure dating of glacially transported boulders on top of the l-LGM moraines. Excluding outliers (see Supplementary Information, Tables S1 and S2), almost all calculated exposure ages fall into the period between 25 and 19 ka (Fig. 3A), demonstrating that l-LGM moraines across the southern Alpine fringe were formed during the g-LGM (26.5 to 19 ka, *sensu* Clark et al., 2009). At four of the seven sites, the data indicate that glaciers had advanced to their l-LGM position by 25 to 24 ka, while moraines at three other sites are related to a later advance, between ca. 20 and 19 ka. At other sites, undated recessional moraines just inside the l-LGM limits may be linked to this second phase of glacier stabilisation at

the end of the g-LGM (cf. Fig. 2). The chronological data from marginal glaciers is consistent with numerical dating from moraine amphitheatres formed by larger outlet glaciers on the southern side of the AIF, which reached their maxima around 26 to 24 ka (Fig. 3B, Monegato et al., 2007; Monegato et al., 2017; Ivy-Ochs et al., 2018; Braakhekke et al., 2020; Kamleitner et al., 2022). Subsequently, these outlet glaciers remained close to their maximum positions until 20 to 19 ka, building sequences of stacked, recessional moraines (Gianotti et al., 2015; Monegato et al., 2017; Braakhekke et al., 2020; Kamleitner et al., 2022; Ribolini et al., 2022b). Widespread moraine formation between ca. 26 and 19 ka, related both to small and large ice masses, implies that the climatic conditions on the southern side of the Alps could sustain glacier growth throughout the entire g-LGM. Proxy records from the foreland plain demonstrate that this period was characterised by a cold and relatively dry climate with annual precipitation sums under 500 mm/yr and July temperatures at sea level not exceeding 12 to 14°C (see Fig. 3C, Samartin et al., 2016; Pini et al., 2022).

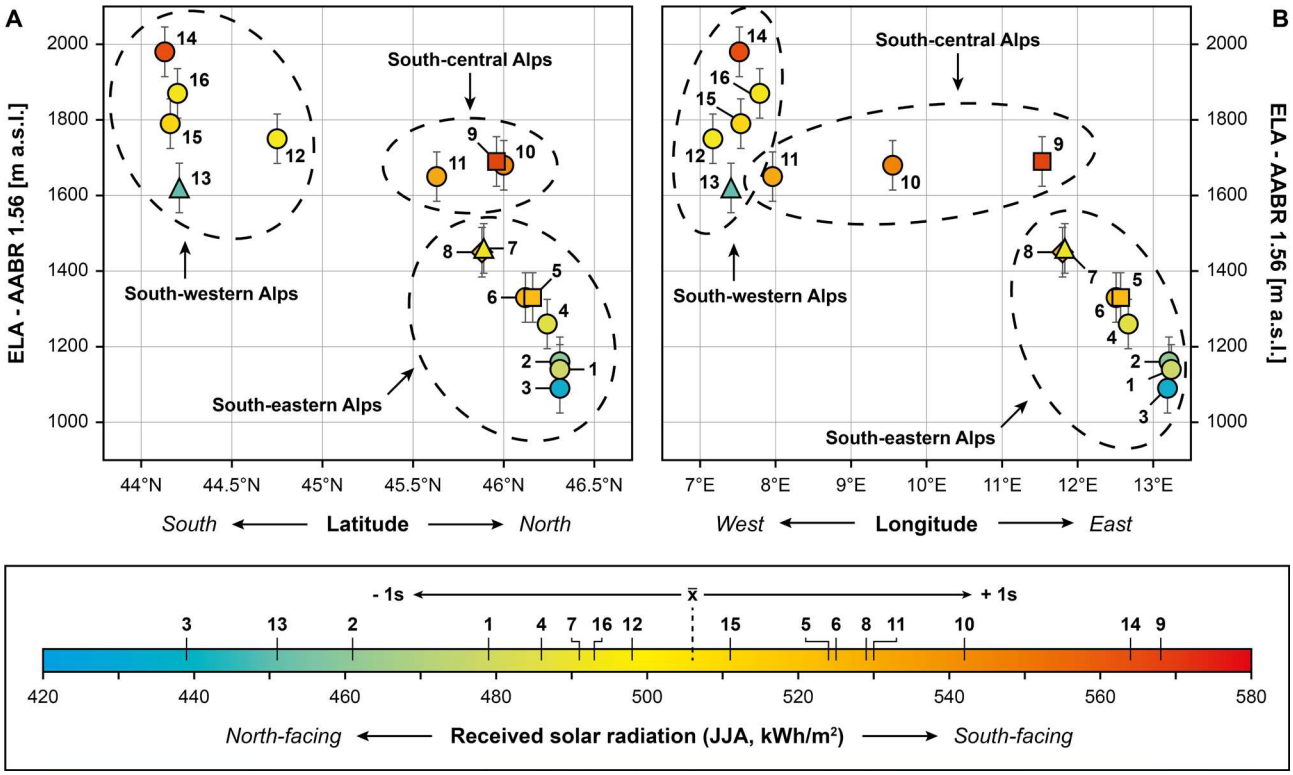


Fig. 4. Reconstructed ELAs of marginal l-LGM glaciers along the southern fringe of the Alps. **A.** ELAs plotted against latitude. **B.** ELAs plotted against longitude. The shape of the symbols refers to the glacier type (see legend in Fig. 1C), while the colour represents the total amount of solar radiation that the reconstructed glacier surfaces would receive in a present-day climate during the summer months of June, July, and August. Numbers 1-16 in all panels refer to Fig. 1C and the Supplementary Information, Table S4.

Palaeoclimate at the ELA

The reconstructed ELAs of marginal l-LGM glaciers are as low as ca. 1100 m a.s.l. in the south-eastern Alps and as high as almost 2000 m a.s.l. in the south-western Alps, with a general trend of decreasing ELAs with increasing latitude and longitude (Fig. 4). Partly, the ELA differences between individual sites can be related

to local variations in catchment aspect that determine the degree to which the ice surfaces were protected from incoming solar radiation. Such aspect-related differences between ELAs can be as high as ca. 400 m in the south-western Alps (Rettig et al., 2024) but are more usually around 100 to 200 m (Fig. 4A, B). For a semi-quantitative evaluation of the influence of catchment aspect on ELAs at the regional scale, we can consider the total amount of incoming radiation that the reconstructed ice surfaces would receive in the present-day climate during the months June, July, and August (G_{JJA}). G_{JJA} varies between ca. 439 and 564 kWh/m^2 with a mean ($\bar{x}$) of 506 kWh/m^2 and a standard error (s) of 37 kWh/m^2 (Fig. 4C). The ELAs for glaciers where G_{JJA} is less than 469 kWh/m^2 ($\bar{x}$-1s, three sites) likely underestimate the true climatic ELA at the time of moraine formation due to high degrees of topographic shading, leading to reduced surface melt and glacier preservation at lower altitudes (Allen, 1998; Coleman et al., 2009; Chandler and Lukas, 2017). ELAs of glaciers where G_{JJA} is greater than 543 kWh/m^2 ($\bar{x}$+1s, two sites), on the other hand, were probably above the true climatic ELA. By discarding these outliers (glaciers no. 2, 3, 9, 13 and 14 in Fig. 4) and considering only those eleven sites at which G_{JJA} is between 469 and 543 kWh/m^2 ($\bar{x}$±1s), we can estimate ELAs that are largely independent of topoclimatic control and therefore representative of the regional climatic conditions.

These climatically representative ELAs, in combination with independent temperature estimates, can be used to obtain quantitative information on LGM precipitation, since empirical data from present-day glaciers demonstrate a link between summer temperature (T_{JJA}) and annual precipitation (P) at the ELA (Ohmura et al., 1992; Golledge et al., 2010; Ohmura and Boettcher, 2018). Here, we retrieved temperature outputs at 21 ka from the RCM by Del Gobbo et al. (2023) and carried out a comprehensive reconstruction of ELA-based palaeoprecipitation (P_{ELA}) for the sites of marginal glaciation. A second RCM (Russo et al., 2024) was then used as a validation of the data and yielded similar results (see Supplementary Information, Table S4). Two different P_{ELA}/T_{JJA} relationships were applied (Fig. 5). Using equation 1 (Ohmura and Boettcher, 2018), computed P_{ELA} is between 1900 ± 680 and 3100 ± 670 mm/yr, with the highest values in the south-eastern Alps, and a gradual lowering moving westward through the south-central to the south-western Alps (Fig. 5A). Notably, P_{ELA} is much higher than precipitation in the present-day climate (Isotta et al., 2014), and at the same time significantly above the precipitation estimates from the RCM itself (P_{RCM}, Del Gobbo et al., 2023): On average the difference between P_{ELA} and P_{RCM} is ca. 960 mm/yr (Fig. 5B). This model-data discrepancy, however, is significantly lower when using a second P_{ELA}/T_{JJA} relationship (Golledge et al., 2010), and by applying a seasonality factor S of 0.8. This seasonality factor implies that precipitation is dominated by the solid fraction, in other words that a large share of precipitation falls on the glacier as snow rather than as rain. Using equation 2 and S = 0.8, calculated P_{ELA} changes to 1100-2400 mm/yr (Fig. 5C). While the regional distribution remains similar, the overall quantities of P_{ELA} are much lower than with equation 1, resulting in a significantly reduced average difference between P_{ELA} and P_{RCM} of 190 mm/yr (Fig. 5D).

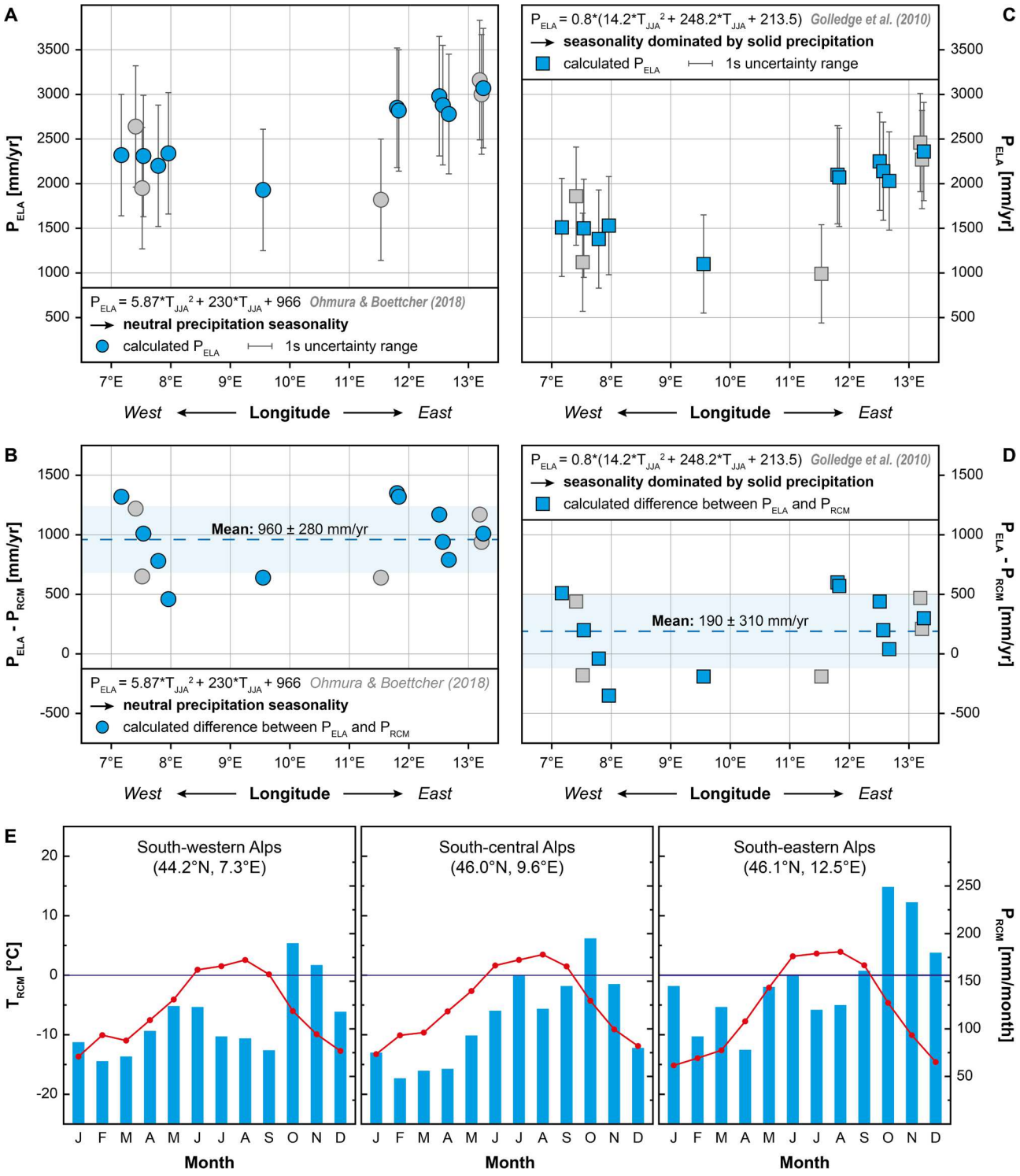


Fig. 5. Reconstructed ELA-based precipitation estimates (P_{ELA}) for the sites of marginal l-LGM glaciation. Grey symbols in panels A to D are related to sites with strong topoclimatic control (see Fig. 4). **A**. P_{ELA} plotted against longitude, using equation 1, the P_{ELA}/T_{JJA}-relationship by Ohmura and Boettcher (2018). **B**. Difference between P_{ELA} and P_{RCM} using equation 1. **C.** P_{ELA} plotted against longitude, using equation 2, the P_{ELA}/T_{JJA}-relationship by Golledge et al. (2010) and a seasonality factor of 0.8. **D**. Difference between P_{ELA} and P_{RCM} using equation 2. Note the much better match between P_{ELA} and P_{RCM} under this second scenario. **E.** Temperature (red line) and precipitation (blue columns) diagrams for the LGM at three representative sites along the southern Alpine fringe, based on monthly RCM data. Note precipitation peaks in autumn and (more subdued) in late spring/early summer. Source of the RCM data: Del Gobbo et al. (2023).

The much-improved fit between P_{ELA} and P_{RCM} when using equation 2 implies that precipitation at the ELAs of marginal glaciers must have occurred predominantly as snow rather than as rain. This is a somewhat surprising finding given that the RCM data show that LGM precipitation peaks did not occur in the winter months but rather in autumn (October/November) and spring to early summer (May-July). However, the model data also indicate that average air temperatures at the ELA in the spring and autumn were still negative and even in the summer months just slightly above 0°C (Fig. 5E). This means that the climate was still cold enough to allow for frequent spring, summer and autumn snowfall events that would have significantly influenced glacier mass balance. Snowfall in late spring and early summer would have increased the albedo, reducing ablation in the summer months (Fujita, 2008; Hughes and Braithwaite, 2008), and autumn snowfall would have resulted in an early build-up of the snowpack and a shortened ablation season, a hypothesis that has previously been suggested based on speleothem data (see Spötl et al., 2021).

Seasonality controls on asynchronous ice advances across Europe

Our findings highlight the importance of precipitation seasonality for the mass balances of marginal l-LGM glaciers in the southern Alps. However, seasonality controls may also explain why mountain glaciers across Europe more broadly responded in different ways to changes in the LGM climatic forcing. Chronological data from several sites in southern Europe and the Mediterranean region, including the southern Balkans (Allard et al., 2020), the central Apennines (Giraudi, 2012, Ribolini et al., 2022a), parts of the Pyrenees (Delmas et al., 2011), and the Anatolian Peninsula (Reber et al., 2014) have suggested that glaciers had already reached their l-LGM positions earlier than the g-LGM. At those sites, the maximum glacier extent during the last glacial cycle occurred either during MIS 3 or during the early part of MIS 2, and generally under more temperate and humid conditions. With the establishment of a colder but drier regional climate after 25 ka, glaciers across the wider Mediterranean region appear to have retreated (Allard et al., 2021).

On the contrary, it is precisely at this time (around 25 ka), when both marginal glaciers along the southern fringe of the Alps and outlet glaciers on the southern side of the AIF reached their maximum extent (Fig. 3, Monegato et al., 2017; Kamleitner et al., 2022), where (albeit with fluctuations) they remained until the end of the g-LGM around 19 ka. In the previous section, we have demonstrated that the mass balances of glaciers in the southern Alps were influenced by spring, summer and autumn snowfall. This also implies that Alpine glaciers were likely very sensitive to small temperature changes, which would have had a relatively large influence on the ratio between liquid and solid precipitation in spring and autumn (Fujita, 2008). In the Mediterranean, on the other hand, precipitation in the present-day climate occurs predominantly in the winter months, and climate models suggest that such seasonality also prevailed during the LGM (e.g., Russo et al., 2024). Sensitivity studies show that the mass balances of glaciers in a climate dominated by winter precipitation are less sensitive to temperature changes (Fujita, 2008). Therefore, at these sites, cooler temperatures after 25 ka could not buffer the effects of increased aridity as they did in the Alps.

Online Methods

Geomorphological mapping and palaeoglacier reconstructions

The reconstructions of l-LGM glacier geometries and their ELAs presented in this study are based on field data from a variety of sites along the southern fringe of the Alps. Some sites in the south-eastern and south-western Alps have previously been discussed in Rettig et al., 2023 and Rettig et al., 2024, while four newly investigated sites in the south-central to south-western Alps are introduced for the first time in the Supplementary Information (Figures S1-S4). All datasets were processed according to a consistent methodological framework. At first, this involved the geomorphological mapping of landforms that delimitate the spatial extent of the former glaciers (e.g., frontal and lateral moraine ridges, trimlines, cirques, kame terraces, or lateral meltwater channels). The mapping was carried out partly from remotely sensed datasets, such as topographic maps, aerial photographs, and Digital Elevation Models (DEMs), and through targeted field surveys during the summers of 2020, 2021, and 2022, largely following the workflow described in Chandler et al. (2018).

The ice-marginal landform assemblage was then digitised in order to constrain numerical reconstructions of former ice surface geometries using GlaRe (Pellitero et al., 2016), an Esri ArcMap toolbox that represents an implementation of the standard flow law of ice (Nye, 1952; Schilling and Hollin, 1981; Benn and Hulton, 2010). GlaRe calculates ice thickness points along user-defined flowlines assuming a perfect plasticity ice rheology and then interpolates these points across the formerly glaciated catchments. This results in a raster file representing the three-dimensional geometry of the palaeoglacier surface. The tool was first run with a default basal shear stress of 100 kPa (Pellitero et al., 2016) after which higher (max. 125 kPa) and/or lower (min. 50 kPa) values were chosen in specific areas in which the first reconstruction did not match the morphological evidence. In particular, lower shear stress values had to be applied in areas of postglacial sediment infill close to the former glacier snouts. Additionally, shape factor (F factor) corrections were used at several sites at which the ice flow was constrained within narrow valleys, as to account for lateral drag from the valley sides (Nye, 1965; Schilling and Hollin, 1981).

From the output ice surface raster files, palaeoglacier ELAs were calculated using the "ELA calculation" toolbox (Pellitero et al., 2015). Both the Area-Altitude Balance Ratio (AABR) method with an AABR of 1.56 (global median value, see Oien et al., 2022) and the Accumulation Area Ratio (AAR) method with an AAR of 0.58 (global median value, see Oien et al., 2022) were applied. At the majority of sites, the differences between AABR- and AAR-ELAs are lower than 50 m (see Supplementary Information, Table S4). Among the few exceptions are glaciers with unusual surface hypsometries such as the Monte Raut Glacier, which has wide and gently sloping accumulation areas and flows through a narrow and steep gorge further down valley (Rettig et al., 2021). As the AABR method specifically accounts for glacier hypsometry (Furbish and Andrews, 1984; Rea, 2009), only AABR-ELAs were therefore used for the subsequent palaeoclimatic analyses.

^{10}Be and ^{36}Cl surface exposure dating

Surface exposure dating using the terrestrial cosmogenic nuclides ^{10}Be and ^{36}Cl was employed to determine the age of l-LGM moraine formation at selected sites (Gosse and Phillips, 2001; Ivy-Ochs and Kober, 2008). Sampling was restricted to erratic boulders that were situated in central and stable positions on well-preserved moraine ridges, avoiding those that appeared to have moved or to have been reworked after deposition (Akçar et al., 2011). The rock samples were collected from flat to moderately inclined boulder surfaces using an angle grinder, hammer, and chisel, and were then crushed to a grain size of <800 μm using a Retsch BB 50 jaw crusher at the Department of Geosciences, University of Padova, Italy. Subsequent chemical processing and Accelerator Mass Spectrometry (AMS) measurements were carried out at the Laboratory of Ion Beam Physics (LIP), ETH Zürich, Switzerland. Boulder and sample properties, as well as shielding

parameters, that were measured and recorded in the field and are listed in the Supplementary Information, Table S1 (^{10}Be data) and Table S2 (^{36}Cl data).

The crushed samples from the Oropa Valley (sample ID: ORO, lithology: gneiss and mica-schist from the Austroalpine Sesia-Lanzo zone), from Pian Frollero (sample ID: FRO, lithology: gneiss from the Penninic Dora-Maira unit), and from Sella Spa (sample ID: COR, lithology: gneiss from the Penninic Briançonnais zone) contained sufficient quantities of quartz to further process them for ^{10}Be dating. The quartz grains were isolated from other minerals using standardised methods (Kohl and Nishiizumi, 1992; Ivy-Ochs, 1996; Ivy-Ochs and Kober, 2008; Kronig et al., 2018), primarily by leaching the material in HCl and several times in weak (4%) HF. Magnetic grains, such as garnet and muscovite, were removed from the mineral assemblage using a Frantz Model L-1 isodynamic separator. Once sufficiently purified, the quartz was spiked with ca. 250 µg of a ^{9}Be carrier and dissolved in concentrated (40%) HF. The dissolved samples were then passed through two sets of ion exchange columns to remove unwanted cations and anions. The addition of a few drops of ammonia solution induced pH-selective precipitation of $Be(OH)_2$, which was oxidized to BeO_2 and pressed into AMS targets. The concentrations of ^{10}Be in the samples were measured using the 0.3 MV MILEA AMS system at LIP (Maxeiner et al., 2019). The measurements were normalised against the internal standard S2007N with a nominal ^{10}Be/^{9}Be ratio of 28.1 x 10^{-12} (Christl et al., 2013) and corrected with a laboratory blank value of $3.18*10^{-15}$. Exposure ages were calculated from the blank-corrected ^{10}Be concentrations using version 2.2 of the online calculators formerly known as the CRONUS-Earth online calculators (Balco et al., 2008, access at https://hess.ess.washington.edu/). We applied the Northeastern North America (NENA) ^{10}Be production rate of 3.87 ± 0.19 atoms*g^{-1}*a^{-1} (Balco et al., 2009), the constant scaling scheme for spallation of Lal (1991) and Stone (2000), and rock surface erosion rates of both 0 and 1 mm/kyr, the latter representing a maximum estimate for crystalline lithologies (André, 2002). The erosion correction increased exposure ages only marginally by 1.5 to 2.0%, which is within the respective internal uncertainties of the measurements.

Due to insufficient quartz yield, the samples from the Inferno Valley (sample IDs: VIF, lithology: South-Alpine Verrucano conglomerate) were processed for whole rock ^{36}Cl dating, following the workflow outlined in Stone et al. (1996), Ivy-Ochs (1996) and Ivy-Ochs et al. (2004). The crushed material was first sieved to a grain size between 250 and 400 µm and then leached with a HNO_3 solution to remove meteoric chlorine. A small fraction of the leached samples was sent to Activation Laboratories Ltd (Ontario, Canada) to determine the concentrations of major and trace elements which are required for the quantification of ^{36}Cl production rates (see Supplementary Information, Table S3). The remaining material (approximately 30 g per sample) was spiked with a ^{35}Cl carrier and dissolved in a mixture of HNO_3 and concentrated HF. $AgNO_3$ was then added to the dissolved samples to induce the precipitation of AgCl, the target material for AMS measurements. Before the samples could be transferred to the AMS, however, they had to be cleaned from the isobar ^{36}S that can cause interference with ^{36}Cl during the measurements. This was achieved by adding $Ba(NO_3)_2$ which caused precipitation of $BaSO_4$ that could be removed from the samples through filtration. The measurements of ^{36}Cl concentrations were performed against the internal K383/4N standard with a nominal ^{36}Cl/Cl ratio of 17.83×10^{-12} using the 6 MV TANDEM facility at LIP (Synal et al., 1997; Christl et al., 2013; Vockenhuber et al., 2019). The internal standard is calibrated against the primary KNSTD5000 standard. Measured ratios were corrected with a laboratory blank of 3.0 x 10^{-15}. Exposure ages were calculated using an in-house spreadsheet based on Alfimov and Ivy-Ochs (2009), which considers the different production pathways of ^{36}Cl through spallation, muon interactions, and low-energy neutron capture. Spallation rates of 48.8 ± 3.4 atoms*gCa^{-1}*a^{-1} (Stone et al., 1996), 162 ± 24 atoms*gK^{-1}*a^{-1} (Evans et al., 1997), 13 ± 3 atoms*gTi^{-1}*a^{-1} (Fink et al., 2000), and 1.9 ± 0.2 atoms*gFe^{-1}*a^{-1} (Stone et al., 2005), and the scaling scheme of Stone (2000) were applied. Analogue to ^{10}Be dating, surface erosion rates of 0 mm/kyr and 1 mm/kyr were used in the

calculation of exposure ages. The erosion correction lowered the ages by ca. 5% for VIF-1 and VIF-3, and by ca. 1% for VIF-2 and VIF-4.

Given the dominance of post-depositional shielding (causing "too young" ages) over inheritance (causing "too old ages") in exposure age datasets, we usually consider the oldest age(s) at a site to most reliably represent the true age of moraine formation (Heyman et al., 2011), especially if those ages were determined from the largest boulders (Heyman et al., 2016). No correction for snow cover was applied, even though the elevation of the boulders allows for limited quantities of snow to persist during the winter months. This is because the true thickness of the snowpack throughout the Holocene and the Late Pleistocene is unknown and because snow cover on top of the sampled boulders was likely much lower than on the ground due to wind-scour effects (cf., Ye et al., 2023).

Assessment of topographic control on glacier ELAs

Glacier mass balance and the elevation of the equilibrium line are primarily determined by (summer) temperature and (annual) precipitation (Ohmura et al., 1992; Ohmura and Boettcher, 2018), but they may also be subject to local topographic control (Allen, 1998; Coleman et al., 2009; Chandler and Lukas, 2017; Hofmann et al., 2024). Catchment aspect can play a particularly important role in this regard: north-facing glaciers that receive less direct incoming solar radiation generally show reduced surface melt and therefore often have lower ELAs than their south-facing counterparts. The differences between ELAs of north- and south-facing glaciers in the same climatic setting can amount to several hundreds of meters (Evans and Cox, 2005). To get a semi-quantitative assessment on the influence of catchment aspect on the palaeoglacier ELAs discussed in this study, incoming solar radiation was computed for all study sites using the "Raster Solar Radiation" tool in Esri ArcGIS Pro 3.3.1, following the procedure outlined in Mills et al. (2012) and Rettig et al. (2024). This tool generates a raster dataset in which each cell value corresponds to the total amount of solar radiation (in kWh/m^2) received over a defined time frame. Here, the time frame was limited to the summer months of June, July, and August, when air temperatures would have been high enough to generate surface melt on the glacier. The output raster datasets were then clipped to the outline of the reconstructed ice surface, and an average radiation value was calculated for each glacier to facilitate a direct comparison between the sites. The modelling of solar radiation was based on present-day (2023) orbital parameters and therefore cannot be considered representative for the LGM in absolute terms. However, since this exercise was carried out to evaluate relative differences between the sites, we regard this difference to be insignificant.

Calculation of LGM precipitation

After having established chronological control and having evaluated the effects of topographic control, the reconstructed ELAs were used to obtain quantitative precipitation estimates (P_{ELA}) for the sites of marginal l-LGM glaciation (see Table S4 for details). Assuming that glaciers were in equilibrium with climate at the time of moraine formation, two empirical relationships between temperature and precipitation at the ELA were applied:

$$P_{ELA} = 5.87T_{JJA}^2 + 230T_{JJA} + 960 \quad \text{(Equation 1)},$$

$$P_{ELA} = S*(14.2T_{JJA}^2 + 248.2T_{JJA} + 213.5) \quad \text{(Equation 2)},$$

where P_{ELA} is the total annual precipitation (liquid + solid) in mm/yr and T_{JJA} is the average air temperature of the three warmest summer months (June, July, and August in the Northern Hemisphere) in °C at the ELA. S is a seasonality factor that is 1 for a neutral precipitation seasonality, 1.4 for a climate dominated by liquid precipitation and 0.8 for a climate dominated by solid precipitation. Equation 1 is from Ohmura and Boettcher (2018) and based on a dataset of around 100 modern glaciers worldwide, for which both mass balance and climatic data are available. Equation 2 is taken from

Golledge et al. (2010) and is based on an analysis of the Younger Dryas glaciation in Scotland. There, the authors found that precipitation seasonality had a strong influence on the ELA, leading them to include a seasonality factor into their P_{ELA}/T_{JJA} relationship.

For both equations, T_{JJA} during the LGM was calculated by first retrieving temperature data for the preindustrial (PI, 1871-1900) from the HISTALP dataset (Auer et al., 2007) and extrapolating them to the glacier ELAs using an altitudinal lapse rate of -0.0065°C/m. Then, an LGM temperature depression DT (PI-LGM) was applied, which was taken from the regional climate model by Del Gobbo et al. (2023). We chose this DT-based approach over taking model-based temperature estimates directly because of the different resolutions between the present-day and the model topography, which would cause larger uncertainties at very small spatial scales. DT (PI-LGM) varies between 5.8 and 7.6°C, which is in good agreement with reconstructions from lowland proxy records in northern Italy (Samartin et al., 2016; Pini et al., 2022), justifying the use of the DT-based approach for the precipitation reconstruction. The calculated P_{ELA} values were finally compared with model-based precipitation estimates (P_{RCM}) both from Del Gobbo et al. (2023) and for validation purposes also with data from another RCM (Russo et al., 2024, see Supplementary Information, Table S5).

We estimated uncertainties in the calculated P_{ELA} values by taking into account (1) the standard deviation of PI temperatures during the period between 1871 and 1900 (0.6-0.8°C, Auer et al., 2007), (2) the median difference between AABR-ELAs and mass-balanced derived ELAs (65.5 m, Oien et al., 2022), and (3) the standard error in the P/T relationships (648 mm/yr, Ohmura and Boettcher, 2018).

Reference list

Akçar, N., Ivy-Ochs, S., Kubik, P.W., Schlüchter, C., 2011. Post-depositional impacts on 'Findlinge' (erratic boulders) and their implications for surface-exposure dating. Swiss Journal of Geosciences, 104, 445-453. https://doi.org/10.1007/s00015-011-0088-7.

Alfimov, V., Ivy-Ochs, S., 2009. How well do we understand production of ^{36}Cl in limestone and dolomite? Quaternary Geochronology, 4 (6), 462-474. https://doi.org/10.1016/j.quageo.2009.08.005.

Allard, J.L., Hughes, P.D., Woodward, J.C., Fink, D., Simon, K., Wilcken, K.M., 2020. Late Pleistocene glaciers in Greece: A new ^{36}Cl chronology. Quaternary Science Reviews, 245, 106528. https://doi.org/10.1016/j.quascirev.2020.106528.

Allard, J. L., Hughes, P. D., Woodward, J. C., 2021. Heinrich Stadial aridity forced Mediterranean-wide glacier retreat in the last cold stage. Nature Geoscience, 14, 197-205. https://doi.org/10.1038/s41561-021-00703-6.

Allen, T.R., 1998. Topographic context of glaciers and perennial snowfields, Glacier National Park, Montana. Geomorphology, 21 (3-4), 207-216. https://doi.org/10.1016/S0169-555X(97)00059-7.

André, M.-F., 2002. Rates of Postglacial rock weathering on glacially scoured outcrops (Abisko-Riksgränsen area, 68°N). Geografiska Annaler: Series A, Physical Geography, 84, 139-150. https://doi.org/10.1111/j.0435-3676.2002.00168.x.

Auer, I., Böhm, R., Jurkovic, A., Lipa, W., Orlik, A., Potzmann, R., Schöner, W., Ungersböck, M., Matulla, C., Briffa, K., Jones, P., Efthymiadis, D., Brunetti, M., Nanni, T., Maugeri, M., Mercalli, L., Mestre, O., Moisselin, J.-M., Begert, M., Müller-Westermeier, G., Kveton, V., Bochnicek, O., Stastny, P., Lapin, M., Szalai, S., Szentimrey, T., Cegnar, T., Dolinar, M., Gajic-Capka, M., Zaninovic, K., Majstorovic, Z., Nieplova, E., 2007. HISTALP - historical instrumental climatological surface time series of the Greater Alpine Region. International Journal of Climatology, 27 (1), 17-46. https://doi.org/10.1002/joc.1377.

Balco, G., Stone, J.O., Lifton, N.A., Dunai, T.J., 2008. A complete and easily accessible means of calculating surface exposure ages or erosion rates from ^{10}Be and ^{26}Al measurements. Quaternary Geochronology, 3 (3), 174-195. https://doi.org/10.1016/j.quageo.2007.12.001.

Balco, G., Briner, J., Finkel, R.C., Rayburn, J.A., Ridge, J.C., Schaefer, J.M., 2009. Regional beryllium-10 production rate calibration for late-glacial northeastern North America. Quaternary Geochronology, 4 (2), 93-107. https://doi.org/10.1016/j.quageo.2008.09.001.

Baratto, A., Ferrarese, F., Meneghel, M., Sauro, U., 2003. La ricostruzione della glaciazione Wurmiana nel Gruppo del Monte Grappa (Prealpi Venete). In: Biancotti, A., Motta, M. (Eds.), Risposta dei processi geomorfologici alle variazioni ambientali, Brigati G., Genova, pp. 67-77.

Benn, D.I., Hulton, N.R.J., 2010. An Excel^{TM} spreadsheet program for reconstructing the surface profile of former mountain glaciers and ice caps. Computers & Geosciences, 36 (5), 605-610. https://doi.org/10.1016/j.cageo.2009.09.016.

Braakhekke, J., Ivy-Ochs, S., Monegato, G., Gianotti, F., Martin, S., Casale, S., Christl, M., 2020. Timing and flow pattern of the Orta Glacier (European Alps) during the Last Glacial Maximum. Boreas, 49 (2), 315-332. https://doi.org/10.1111/bor.12427.

Carraro, F., Sauro, U., 1979. Il glacialismo "locale" Würmiano del Massiccio del Grappa (Provincie di Treviso e di Vicenza). Geografia Fisica e Dinamica Quaternaria, 2 (1), 6-16. https://www.gfdq.glaciologia.it/index.php/GFDQ/article/view/1026.

Chandler, B.M., Lukas, S., 2017. Reconstruction of Loch Lomond Stadial (Younger Dryas) glaciers on Ben More Coigach, north-west Scotland, and implications for reconstructing palaeoclimate using small ice masses. Journal of Quaternary Science, 32 (4), 475-492. https://doi.org/10.1002/jqs.2941.

Chandler, B.M.P., Lovell, H., Boston, C.M., Lukas, S., Barr, I.D., Benediktsson, Í.Ö., Benn, D.I., Clark, C.D., Darvill, C.M., Evans, D.J.A., Ewertowski, M.W., Loibl, D., Margold, M., Otto, J.-C., Roberts, D.H., Stokes, C.R., Storrar, R.D., Stroeven, A.P., 2018. Glacial geomorphological mapping: A review of approaches and frameworks for best practice. Earth-Science Reviews, 185, 806-846. https://doi.org/10.1016/j.earscirev.2018.07.015.

Christl, M., Vockenhuber, C., Kubik, P.W., Wacker, L., Lachner, J., Alfimov, V., Synal, H.-A., 2013. The ETH Zurich AMS facilities: Performance parameters and reference materials. Nuclear Instruments and Methods in Physics Research Section B: Beam Interactions with Materials and Atoms, 294, 29-38. https://doi.org/10.1016/j.nimb.2012.03.004.

Clark, P.U., Dyke, A.S., Shakun, J.D., Carlson, A.E., Clark, J., Wohlfarth, B., Mitrovica, J.X., Hostetler, S.W., McCabe, A.M., 2009. The Last Glacial Maximum. Science, 325 (5941), 710-714. https://doi.org/10.1126/science.1172873.

Coleman, C.G., Carr, S.J., Parker, A.G., 2009. Modelling topoclimatic controls on palaeoglaciers: implications for inferring palaeoclimate from geomorphic evidence. Quaternary Science Reviews, 28 (3-4), 249-259. https://doi.org/10.1016/j.quascirev.2008.10.016.

Del Gobbo, C., Colucci, R.R., Monegato, G., Žebre, M., Giorgi, F., 2023. Atmosphere-cryosphere interactions during the last phase of the Last Glacial Maximum (21 ka) in the European Alps. Climate of the Past, 19 (9), 1805-1823. https://doi.org/10.5194/cp-19-1805-2023.

Delmas, M., Calvet, M., Gunnell, Y., Braucher, R., Bourlès, D., 2011. Palaeogeography and ^{10}Be exposure-age chronology of Middle and Late Pleistocene glacier systems in the northern Pyrenees: Implications for reconstructing regional palaeoclimates. Palaeogeography, Palaeoclimatology, Palaeoecology, 305 (1-4), 109-122. https://doi.org/10.1016/j.palaeo.2011.02.025.

Ehlers, J., Gibbard, P.L., Hughes, P.D. (Eds.), 2011. Quaternary Glaciations - Extent and Chronology - A Closer Look. Developments in Quaternary Science, 15. Elsevier, Amsterdam, 1108 pp.

Engel, Z., Mentlík, P., Braucher, R., Minár, J., Léanni, L., ASTER Team, 2015. Geomorphological evidence and ^{10}Be exposure ages for the Last Glacial Maximum and deglaciation of the Velká and Malá Studená dolina valleys in the High Tatra Mountains, central Europe. Quaternary Science Reviews, 124, 106-123. https://doi.org/10.1016/j.quascirev.2015.07.015.

Evans, I.S., Cox, N.J., 2005. Global variations of local asymmetry in glacier altitude: separation of north-south and east-west components. Journal of Glaciology, 51 (174), 469-482. https://doi.org/10.3189/172756505781829205.

Evans, J.M., Stone, J.O.H., Fifield, L.K., Cresswell, R.G., 1997. Cosmogenic chlorine-36 production in K-feldspar. Nuclear Instruments and Methods in Physics Research Section B: Beam Interactions with Materials and Atoms, 123 (1-4), 334-340. https://doi.org/10.1016/S0168-583X(96)00714-8.

Fink, D., Vogt, S., Hotchkis, M., 2000. Cross-sections for ^{36}Cl from Ti at E_p=35-150 MeV: Applications to in-situ exposure dating. Nuclear Instruments and Methods in Physics Research Section B: Beam Interactions with Materials and Atoms, 172 (1-4), 861-866. https://doi.org/10.1016/S0168-583X(00)00200-7.

Forno, M.G., Gianotti, F., Racca, G., 2010. Significato paleoclimatico dei rapporti tra il glacialismo principale e quello tributario nella bassa valle della Dora Baltea. Il Quaternario - Italian Journal of Quaternary Sciences, 23 (1), 105-124. https://amq.aiqua.it/index.php/amq/article/view/289.

Fujita, K., 2008. Effect of precipitation seasonality on climatic sensitivity of glacier mass balance. Earth and Planetary Science Letters, 276 (1-2), 14-19. https://doi.org/10.1016/j.epsl.2008.08.028.

Furbish, D.J., Andrews, J.T., 1984. The Use of Hypsometry to Indicate Long-Term Stability and Response of Valley Glaciers to Changes in Mass Transfer. Journal of Glaciology, 30 (105), 199-211. https://doi.org/10.3189/S0022143000005931.

Gianotti, F., Forno, M.G., Ivy-Ochs, S., Monegato, G., Pini, R., Ravazzi, C., 2015. Stratigraphy of the Ivrea morainic amphitheatre (NW Italy): An updated synthesis. Alpine and Mediterranean Quaternary, 28 (1), 29-58. https://amq.aiqua.it/index.php/amq/article/view/80.

Gillespie, A., Molnar, P., 1995. Asynchronous maximum advances of mountain and continental glaciers. Reviews of Geophysics, 33 (3), 311-364. https://doi.org/10.1029/95RG00995.

Giorgi, F., Coppola, E., Solmon, F., Mariotti, L., Sylla, M.B., Bi, X., Elguindi, N., Diro, G.T., Nair, V., Giuliani, G., Turuncoglu, U.U., Cozzini, S., Güttler, I., O'Brien, T.A., Tawfik, A.B., Shalaby, A., Zakey, A.S., Steiner, A.L., Stordal, F., Sloan, L.C., Brankovic, C., 2012. RegCM4: model description and preliminary tests over multiple CORDEX domains. Climate Research, 52, 7-29. https://doi.org/10.3354/cr01018.

Giraudi, C., 2012. The Campo Felice late Pleistocene Glaciation (Apennines, central Italy). Journal of Quaternary Science, 27 (4), 432-440. https://doi.org/10.1002/jqs.1569.

Golledge, N., Hubbard, A., Bradwell, T., 2010. Influence of seasonality on glacier mass balance, and implications for palaeoclimate reconstructions. Climate Dynamics, 35, 757-770. https://doi.org/10.1007/s00382-009-0616-6.

Gosse, J.C., Phillips, F.M., 2001. Terrestrial in situ cosmogenic nuclides: theory and application. Quaternary Science Reviews, 20 (14), 1475-1560. https://doi.org/10.1016/S0277-3791(00)00171-2.

Heyman, J., Stroeven, A.P., Harbor, J.M., Caffee, M.W., 2011. Too young or too old: Evaluating cosmogenic exposure dating based on an analysis of compiled boulder exposure ages. Earth and Planetary Science Letters, 302 (1-2), 71-80. https://doi.org/10.1016/j.epsl.2010.11.040.

Heyman, J., Applegate, P.J., Blomdin, R., Gribenski, N., Harbor, J.M., Stroeven, A.P., 2016. Boulder height - exposure age relationships from a global glacial ^{10}Be compilation. Quaternary Geochronology, 34, 1-11. https://doi.org/10.1016/j.quageo.2016.03.002.

Hock, R., Rasul, G., Adler, C., Cáceres, B., Gruber, S., Hirabayashi, Y., Jackson, M., Kääb, A., Kang, S., Kutuzov, S., Milner, A., Molau, U., Morin, S., Orlove, B., Steltzer, H., 2019. High Mountain Areas. In: Pörtner, H.-O., Roberts, D.C., Masson-Delmotte, V., Zhai, P., Tignor, M., Poloczanska, E., Mintenbeck, K., Alegría, A., Nicolai, M., Okem, A., Petzold, J., Rama, B., Weyer, N.M. (Eds.), IPCC Special Report on the Ocean and Cryosphere in a Changing Climate, Cambridge University Press, Cambridge, UK and New York, USA, pp. 131-202. https://doi.org/10.1017/9781009157964.004.

Hofmann, F.M., Steiner, M., Hergarten, S., Preusser, F., ASTER Team, 2024. Limitations of precipitation reconstructions using equilibrium-line altitudes exemplified for former glaciers in the Southern Black Forest, Central Europe. Quaternary Research, 117, 135-159. https://doi.org/10.1017/qua.2023.53.

Hughes, P.D., Braithwaite, R.J., 2008. Application of a degree-day model to reconstruct Pleistocene glacial climates. Quaternary Research, 69 (1), 110-116. https://doi.org/10.1016/j.yqres.2007.10.008.

Hughes, P.D., Gibbard, P.L., Ehlers, J., 2013. Timing of glaciation during the last glacial cycle: evaluating the concept of a global 'Last Glacial Maximum' (LGM). Earth-Science Reviews, 125, 171-198. https://doi.org/10.1016/j.earscirev.2013.07.003.

Isotta, F.A., Frei, C., Weilguni, V., Perčec Tadić, M., Lassegues, P., Rudolf, B., Pavan, V., Cacciamani, C., Antolini, G., Ratto, S.M., Munari, M., Micheletti, S., Bonati, V., Lussana, C., Ronchi, C., Panettieri, E., Marigo, G., Vertačnik, G., 2014. The climate of daily precipitation in the Alps: development and analysis of a high-resolution grid dataset from pan-Alpine rain-gauge data. International Journal of Climatology, 34 (5), 1657-1675. https://doi.org/10.1002/joc.3794.

Ivy-Ochs, S., 1996. The dating of rock surfaces using in situ produced ^{10}Be, ^{26}Al and ^{36}Cl, with examples from Antarctica and the Swiss Alps. Ph.D. dissertation, ETH Zürich, 210 pp. https://doi.org/10.3929/ethz-a-001772745.

Ivy-Ochs, S., Synal, H.-A., Roth, C., Schaller, M., 2004. Initial results from isotope dilution for Cl and ^{36}Cl measurements at the PSI/ETH Zurich AMS facility. Nuclear Instruments and Methods in Physics Research Section B: Beam Interactions with Materials and Atoms, 223-224, 623-627. https://doi.org/10.1016/j.nimb.2004.04.115.

Ivy-Ochs, S., Kober, F., 2008. Surface exposure dating with cosmogenic nuclides. E&G Quaternary Science Journal, 57 (1/2), 179-209. https://doi.org/10.3285/eg.57.1-2.7.

Ivy-Ochs, S., Lucchesi, S., Baggio, P., Fioraso, G., Gianotti, F., Monegato, G., Graf, A.A., Akçar, N., Christl, M., Carraro, F., Forno, M.G., Schlüchter, C., 2018. New geomorphological and chronological constraints for glacial deposits in the Rivoli-Avigliana end-moraine system and the lower Susa Valley (Western Alps, NW Italy). Journal of Quaternary Science, 33 (5), 550-562. https://doi.org/10.1002/jqs.3034.

Jouvet, G., Cohen, D., Russo, E., Buzan, J., Raible, C.C., Haeberli, W., Kamleitner, S., Ivy-Ochs, S., Imhof, M.A., Becker, J.K., Landgraf, A., Fischer, U.H., 2023. Coupled climate-glacier modelling of the last glaciation in the Alps. Journal of Glaciology, 69 (278), 1956-1970. https://doi.org/10.1017/jog.2023.74.

Kamleitner, S., Ivy-Ochs, S., Monegato, G., Gianotti, F., Akçar, N., Vockenhuber, C., Christl, M., Synal, H.-A., 2022. The Ticino-Toce glacier system (Swiss-Italian Alps) in the framework of the Alpine Last Glacial Maximum. Quaternary Science Reviews, 279, 107400. https://doi.org/10.1016/j.quascirev.2022.107400.

Kohl, C.P., Nishiizumi, K., 1992. Chemical isolation of quartz for measurement of in-situ-produced cosmogenic nuclides. Geochimica et Cosmochimica Acta, 56 (9), 3583-3587. https://doi.org/10.1016/0016-7037(92)90401-4.

Kronig, O., Ivy-Ochs, S., Hajdas, I., Christl, M., Wirsig, C., Schlüchter, C., 2018. Holocene evolution of the Triftje- and the Oberseegletscher (Swiss Alps) constrained with ^{10}Be exposure and radiocarbon dating. Swiss Journal of Geosciences, 111, 117-131. https://doi.org/10.1007/s00015-017-0288-x.

Lal, D., 1991. Cosmic ray labeling of erosion surfaces: in situ nuclide production rates and erosion models. Earth and Planetary Science Letters, 104 (2-4), 424-439. https://doi.org/10.1016/0012-821X(91)90220-C.

Lambeck, K., Rouby, H., Purcell, A., Sambridge, M., 2014. Sea level and global ice volumes from the Last Glacial Maximum to the Holocene. Proceedings of the National Academy of Sciences of the United States of America, 111 (43), 15296-15303. https://doi.org/10.1073/pnas.1411762111.

Leger, T.P.M., Jouvet, G., Kamleitner, S., Mey, J. Herman, F., Finley, B.D., Ivy-Ochs, S., Vieli, A., Henz, A., Nussbaumer, S.U., 2025. A data-consistent model of the last glaciation in the Alps achieved with physics-driven AI. Nature Communications, 16, 848. https://doi.org/10.1038/s41467-025-56168-3.

López-Moreno, J.I., García-Ruiz, J.M., 2025. Discrepancies in dating the expansion of European glaciers during the Last Glacial Cycle. Geomorphology, 471, 109566. https://doi.org/10.1016/j.geomorph.2024.109566.

Mackintosh, A.N., Anderson, B.M., Pierrehumbert, R.T., 2017. Reconstructing climate from glaciers. Annual Review of Earth and Planetary Sciences, 45, 649-680. https://doi.org/10.1146/annurev-earth-063016-020643.

Makos, M., Rinterknecht, V., Braucher, R., Tołoczko-Pasek, A., Arnold, M., Aumaître, G., Bourlès, D., Keddadouche, K., ASTER Team, 2018. Last Glacial Maximum and Lateglacial in the Polish High Tatra Mountains - Revised

524 deglaciation chronology based on the ^{10}Be exposure age dating. Quaternary Science Reviews, 187, 130-156.
525 https://doi.org/10.1016/j.quascirev.2018.03.006.
526 Maxeiner, S., Synal, H.-A., Christl, M., Suter, M., Müller, A., Vockenhuber, C., 2019. Proof-of-principle of a compact
527 300 kV multi-isotope AMS facility. Nuclear Instruments and Methods in Physics Research Section B: Beam
528 Interactions with Materials and Atoms, 439, 84-89. https://doi.org/10.1016/j.nimb.2018.11.028.
529 Mills, S.C., Grab, S.W., Rea, B.R., Carr, S.J., Farrow, A., 2012. Shifting westerlies and precipitation patterns during the
530 Late Pleistocene in southern Africa determined using glacier reconstruction and mass balance modelling.
531 Quaternary Science Reviews, 55, 145-159. https://doi.org/10.1016/j.quascirev.2012.08.012.
532 Monegato, G., Ravazzi, C., Donegana, M., Pini, R., Calderoni, G., Wick, L., 2007. Evidence of a two-fold glacial
533 advance during the last glacial maximum in the Tagliamento end moraine system (eastern Alps). Quaternary
534 Research, 68 (2), 284-302. https://doi.org/10.1016/j.yqres.2007.07.002.
535 Monegato, G., 2012. Local glaciers in the Julian Prealps (NE Italy) during the Last Glacial Maximum. Alpine and
536 Mediterranean Quaternary, 25, 5-14. https://amq.aiqua.it/index.php/amq/article/view/40.
537 Monegato, G., Scardia, G., Hajdas, I., Rizzini, F., Piccin, A., 2017. The Alpine LGM in the boreal ice-sheets game.
538 Scientific Reports, 7, 2078. https://doi.org/10.1038/s41598-017-02148-7.
539 Nye, J.F., 1952. A Method of Calculating the Thicknesses of the Ice-Sheets. Nature, 169, 529-530.
540 https://doi.org/10.1038/169529a0.
541 Nye, J.F., 1965. The Flow of a Glacier in a Channel of Rectangular, Elliptic or Parabolic Cross-Section. Journal of
542 Glaciology, 5 (41), 661-690. https://doi.org/10.3189/S0022143000018670.
543 Ohmura, A., Kasser, P., Funk, M., 1992. Climate at the Equilibrium Line of Glaciers. Journal of Glaciology, 38 (130),
544 397-411. https://doi.org/10.3189/S0022143000002276.
545 Ohmura, A., Boettcher, M., 2018. Climate on the equilibrium line altitudes of glaciers: theoretical background behind
546 Ahlmann's P/T diagram. Journal of Glaciology, 64 (245), 489-505. https://doi.org/10.1017/jog.2018.41.
547 Oien, R.P., Rea, B.R., Spagnolo, M., Barr, I.D., Bingham, R.G., 2022. Testing the area-altitude balance ratio (AABR)
548 and accumulation-area ratio (AAR) methods of calculating glacier equilibrium-line altitudes. Journal of Glaciology,
549 68 (268), 357-368. https://doi.org/10.1017/jog.2021.100.
550 Palacios, D., Hughes, P.D., García-Ruiz, J.M., Andrés, N. (Eds.), 2021. European Glacial Landscapes: Maximum
551 Extent of Glaciations. Elsevier, Amsterdam, 528 pp.
552 Pellitero, R., Rea, B.R., Spagnolo, M., Bakke, J., Hughes, P., Ivy-Ochs, S., Lukas, S., Ribolini, A., 2015. A GIS tool for
553 automatic calculation of glacier equilibrium-line altitudes. Computers & Geosciences, 82, 55-62.
554 https://doi.org/10.1016/j.cageo.2015.05.005.
555 Pellitero, R., Rea, B.R., Spagnolo, M., Bakke, J., Ivy-Ochs, S., Frew, C.R., Hughes, P., Ribolini, A., Lukas, S., Renssen,
556 H., 2016. GlaRe, a GIS tool to reconstruct the 3D surface of palaeoglaciers. Computers & Geosciences, 94, 77-85.
557 https://doi.org/10.1016/j.cageo.2016.06.008.
558 Pini, R., Furlanetto, G., Vallé, F., Badino, F., Wick, L., Anselmetti, F.S., Bertuletti, P., Fusi, N., Morlock, M.A.,
559 Delmonte, B., Harrison, S.P., Maggi, V., Ravazzi, C., 2022. Linking North Atlantic and Alpine Last Glacial
560 Maximum climates via a high-resolution pollen-based subarctic forest steppe record. Quaternary Science Reviews,
561 294, 107759. https://doi.org/10.1016/j.quascirev.2022.107759.
562 Rea, B.R., 2009. Defining modern day Area-Altitude Balance Ratios (AABRs) and their use in glacier-climate
563 reconstructions. Quaternary Science Reviews, 28 (3-4), 237-248. https://doi.org/10.1016/j.quascirev.2008.10.011.

Reber, R., Akçar, N., Yesilyurt, S., Yavuz, V., Tikhomirov, D., Kubik, P.W., Schlüchter, C., 2014. Glacier advances in northeastern Turkey before and during the global Last Glacial Maximum. Quaternary Science Reviews, 101, 177-192. https://doi.org/10.1016/j.quascirev.2014.07.014.

Rettig, L., Monegato, G., Mozzi, P., Žebre, M., Casetta, L., Fernetti, M., Colucci, R.R., 2021. The Pleistocene evolution and reconstruction of LGM and Late Glacial paleoglaciers of the Silisia Valley and Mount Raut (Carnic Prealps, NE-Italy). Alpine and Mediterranean Quaternary, 34, 277-290. https://amq.aiqua.it/index.php/amq/article/view/375.

Rettig, L., Monegato, G., Spagnolo, M., Hajdas, I., Mozzi, P., 2023. The Equilibrium Line Altitude of isolated glaciers during the Last Glacial Maximum - New insights from the geomorphological record of the Monte Cavallo Group (south-eastern European Alps). Catena, 229, 107187. https://doi.org/10.1016/j.catena.2023.107187.

Rettig, L., Kamleitner, S., Mozzi, P., Ribolini, A., Ivy-Ochs, S., Rea, B.R., Monegato, G., Christl, M., Spagnolo, M., 2024. Responses of small mountain glaciers in the Maritime Alps (South-Western European Alps) to climatic changes during the Last Glacial Maximum. Quaternary Science Reviews, 325, 108484. https://doi.org/10.1016/j.quascirev.2023.108484.

Reuther, A.U., Fiebig, M., Ivy-Ochs, S., Kubik, P.W., Reitner, J.M., Jerz, H., Heine, K., 2011. Deglaciation of a large piedmont lobe glacier in comparison with a small mountain glacier – new insight from surface exposure dating. Two studies from SE Germany. E&G Quaternary Science Journal, 60 (2/3), 18. https://doi.org/10.3285/eg.60.2-3.03.

Ribolini, A., Spagnolo, M., Giraudi, C., 2022a. The Italian mountains: glacial landforms from the Last Glacial Maximum. In: Palacios, D., Hughes, P.D, García-Ruiz, J.M., Andrés N. (Eds.), European Glacial Landscapes. Elsevier, Amsterdam, pp. 481-486. https://doi.org/10.1016/B978-0-12-823498-3.00022-4.

Ribolini, A., Spagnolo, M., Cyr, A.J., Federici, P.R., 2022b. Last Glacial Maximum and early deglaciation in the Stura Valley, southwestern European Alps. Quaternary Science Reviews, 295, 107770. https://doi.org/10.1016/j.quascirev.2022.107770.

Russo, E., Buzan, J., Lienert, S., Jouvet, G., Velasquez Alvarez, P., Davis, B., Ludwig, P., Joos, F., Raible, C.C., 2024. High-resolution LGM climate of Europe and the Alpine region using the regional climate model WRF. Climate of the Past, 20 (3), 449-465. https://doi.org/10.5194/cp-20-449-2024.

Samartin, S., Heiri, O., Kaltenrieder, P., Kühl, N., Tinner, W., 2016. Reconstruction of full glacial environments and summer temperatures from Lago della Costa, a refugial site in Northern Italy. Quaternary Science Reviews, 143, 107-119. https://doi.org/10.1016/j.quascirev.2016.04.005.

Schilling, D.H., Hollin, J.T., 1981. Numerical reconstructions of valley glaciers and small ice caps. In: Denton, G.H., Hughes, T.J. (Eds.), The Last Great Ice Sheets. Wiley, New York, pp. 207-220.

Spötl, C., Koltai, G., Jarosch, A.H., Cheng, H., 2021. Increased autumn and winter precipitation during the Last Glacial Maximum in the European Alps. Nature Communications, 12, 1839. https://doi.org/10.1038/s41467-021-22090-7.

Stone, J.O., Allan, G.L., Fifield, L.K., Cresswell, R.G., 1996. Cosmogenic chlorine-36 from calcium spallation. Geochimica et Cosmochimica Acta, 60 (4), 679-692. https://doi.org/10.1016/0016-7037(95)00429-7.

Stone, J.O., 2000. Air pressure and cosmogenic isotope production. Journal of Geophysical Research: Solid Earth, 105 (B10), 23753-23759. https://doi.org/10.1029/2000JB900181.

Stone, J.O., Fifield, K., Vasconcelos, P., 2005. Terrestrial chlorine-36 production from spallation of iron. In: Abstract of 10th International Conference on Accelerator Mass Spectrometry. Berkeley, California, USA.

Synal, H.-A., Bonani, G., Döbeli, M., Ender, R.M., Gartenmann, P., Kubik, P.W., Schnabel, C., Suter, M., 1997. Status report of the PSI/ETH AMS facility. Nuclear Instruments and Methods in Physics Research Section B: Beam Interactions with Materials and Atoms, 123 (1-2), 62-68. https://doi.org/10.1016/S0168-583X(96)00608-8.

Vockenhuber, C., Miltenberger, K.-U., Synal, H.-A., 2019. ^{36}Cl measurements with a gas-filled magnet at 6 MV. Nuclear Instruments and Methods in Physics Research Section B: Beam Interactions with Materials and Atoms, 455, 190-194. https://doi.org/10.1016/j.nimb.2018.12.046.

Ye, S., Cuzzone, J.K., Marcott, S.A., Licciardi, J.M., Ward, D.J., Heyman, J., Quinn, D.P., 2023. A quantitative assessment of snow shielding effects on surface exposure dating from a western North American ^{10}Be data compilation. Quaternary Geochronology, 76, 101440. https://doi.org/10.1016/j.quageo.2023.101440.

Supplementary Files

This is a list of supplementary files associated with this preprint. Click to download.

- Rettigetal2026NatureGeoscienceSupplements.pdf